Giving Arthritis the Finger: Customized Medical Device, Optimized for Durability

*Keywords: Medical Device, Customized Medicine, Arthritis, CT, MRI, DICOM, Simpleware, ScanIP, CAD, CATIA, **3D**EXPERIENCE, FEA, Finite Element Analysis, Abaqus, fatigue, fe-safe, fe-safe/rubber, Endurica, Rubber, Shape Optimization, Tosca, FDA, EMEA*

Abstract

Rheumatoid arthritis is an autoimmune disorder that frequently affects the fingers and results in swollen and/or painful joints. Total joint replacement surgery is commonly required, in which a silicone elastomer prosthetic is implanted to restore patient hand/finger function and alleviate pain. Design qualification requirements specify that the prosthetic must endure at least 10 million cycles in which the finger joint is flexed through 90 degrees, which is typically determined and verified through a battery of costly physical testing routines [4]. However, physics-based simulation is becoming a commonly used method as an enhancement or replacement to physical testing by medical device companies to save time and money when submitting a device for approval to the US Food and Drug Administration (FDA) and the European Medicines Evaluation Agency (EMEA). The workflow presented here describes why and how to leverage patient-specific anatomical data, non-linear structural simulation, fatigue simulation and shape optimization to generate a customized simulation workflow to enhance device design of a total finger joint replacement.

Standard treatment consists of removing the joint tissue and replacing with an off the shelf prosthetic. This workflow aims to customize both the implant and the excised joint tissue. The simulation starts with a patient-specific CT scan of the hand which is parsed by density into various tissue types. With the geometric boundaries established for the tissues the implant is aligned with the anatomy and a boolean operation is performed to remove the tissue occupying the same space as the implant. In order to optimize the prosthetic and ensure compliance to the durability specification, a non-linear finite element model is created of the proposed treatment plan and of typical post-treatment duty cycle of the finger joint. Stress-strain behavior for the silicone elastomer is represented via a 3rd order Ogden hyperelastic law. Fracture mechanics behavior is defined via a non-crystallizing Thomas law. Durability calculations are made via Critical Plane Analysis to address the multiaxiality of loads experienced by the implant. The calculation returns the number of duty cycle repeats required to grow a crack precursor from its naturally occurring initial size to its end-of-life size. Shape optimization is then used to both modify the tissue removal and the prosthetic shape to maximize the durability and provide the best patient outcome.

Introduction

Rheumatoid arthritis can affect man joins of the body however for this study we will limit the scope to the fingers or phalanges. In a typical hand there are 27 bones. Each finger has proximal intermediate and distal phalanges. The thumbs do not have intermediate phalanges. A schematic of the hand is shown in Figure 1.

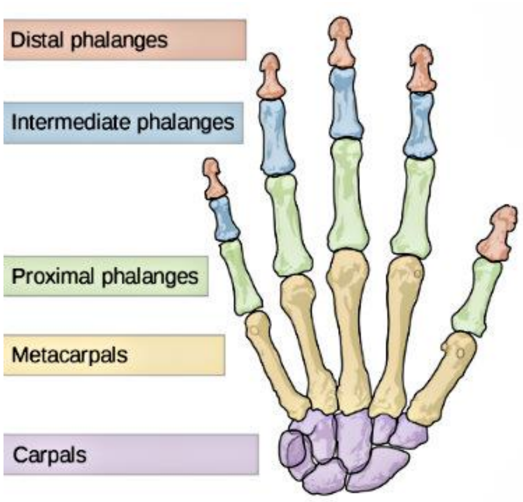

Figure 1 Bones of the hand

Each of these joints share many similarities with each other and are predominately different in size. When considering the full population range the differences between an index and middle finger seem minor. For this study we will look at each joint and across the population range as a single design space with similar design variables and inputs along with patient outcome parameters.

This design is loosely based on the SWANSON Finger Joint Implant which is a “flexible intramedullary-stemmed one-piece implant developed as an adjunct to resection arthroplasty”.[1]

Figure 2 SWANSON Finger Joint Implant

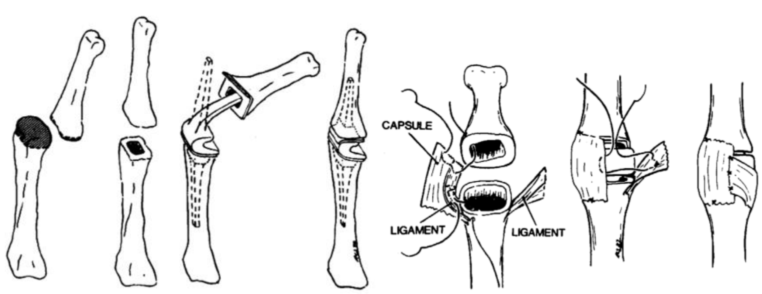

Figure 3 Surgical technique

Model

CT Reconstruction (ScanIP)

Clinical Computed Tomography (CT) scan data of the right hand from the Visible Korean dataset and was used for this project. Clinical CT data is provided in the DICOM format, which is essentially a stack of 2D grey scale images over a 3D volume. The Visible Korean project provides an open source data repository of MRIs, CTs, sectioned images and pre-segmented images which are intended to be the source of virtual dissection, operations etc. to contribute in the medical, informatics, and industrial fields. To achieve the purpose, an average Korean male cadaver (33 years old, 1.64m, 55kg), who died of leukemia on March 26th, 2001, was used.[1] For the current study, the hand was in the neutral position with the fingers extended. Synopsys' Simpleware™ ScanIP software (Synopsys Inc., Mountain View, CA) was used to process the Visible Korean Data and convert the CT images from voxels, which are 3D pixels or volumetric pixels, to a tessellated surface representation in the STL format (Stereolithography) which is an unstructured triangular mesh of points and connectivity. Below is a rough step by step order of operations.

DICOM CT image data imported into Simpleware.

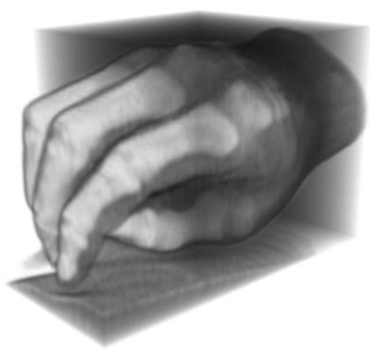

Figure 4 Visible Korean CT scan of hand viewed in Simpleware

The hand was scanned in roughly a neutral hand position similar to the image below of a hand on an ergonomic mouse

Figure 5 Hand on ergonomic mouse. Photo credit, Rob Stupplebeen's left hand; hand model, Rob Stupplebeen's right hand.

Bone tissue was separated from the surrounding soft tissue based on gray scale intensity. This method was able to create voxel groups of the bones of the hand

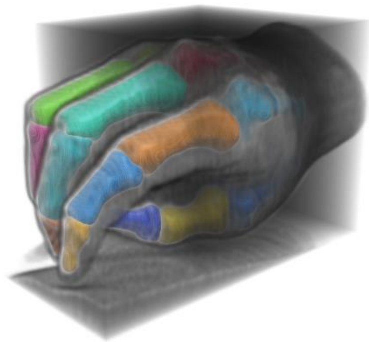

Figure 6 Voxel group of the bones of the hand with CT data overlaid

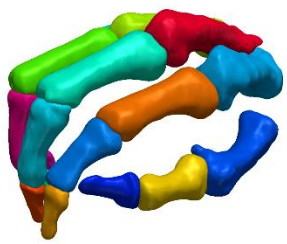

Figure 7 Bones of the hand partitioned from the soft tissue

These bones were exported as an STL.

Computer Aided Design CAD (CATIA)

The individual STLs were imported into the 3DExpereince as point clouds with CATIA's Digitized Shape Preparation.

Figure 8 Imported STLs in CATIA

A parametric CAD model was created for the prosthetic. This geometry is not mean to replicate a commercially available product or imply its performance. Due to the organic nature of the design surface based modelling techniques were used. Care was also given to assure a design which is curvature continuous to reduce any stress risers and to provide smooth geometry for the shape optimization to begin with. The middle metacarpal and proximal phalange or the first joint of the middle finger is the focus of this study.

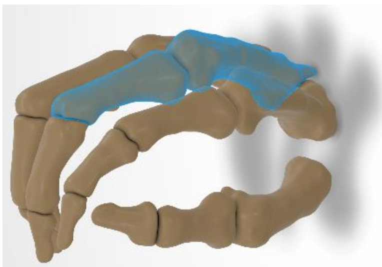

Figure 9 Middle metacarpal and proximal phalange isolated

The custom implant is to be designed in place on top of the scan data. To begin, a coordinate system needed to be developed along with reference geometry. 3 points were created for the point of contact of the joint and the most distal and proximal points. These created an initial coordinate system and by extruding surface cylinders and viewing the model with reference to this coordinate system the initial points can be refined iteratively.

Figure 10 A coordinate system was setup by creating points, planes and cylinders

The implant geometry is a simplified design representative of an actual implant. It consists of an extruded taco shape with 2 tapering stems that will insert into the reamed interamedullary canal.

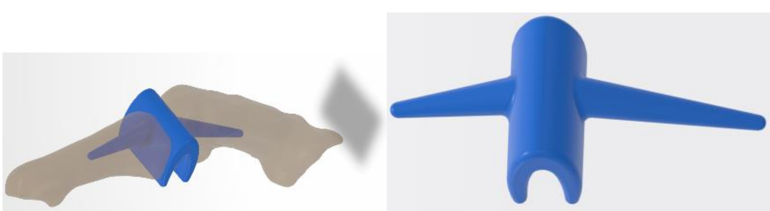

Figure 11 Implant design

CATIA's Digitized Shape to Surface app was used to wrap NURBS (Non-uniform rational basis spline) surface geometry around the point cloud. CATIA's Generative Surface Design was used to design the device and cut the bone geometry similar to how the surgeon would resect the joint and ream the intramedullary canal.

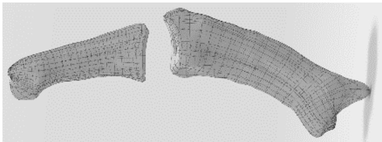

Figure 12 Solid CAD geometry of bones after tissue has been removed.

Figure 13 Implant and prepared tissue

The implant and the 2 prepared bones are exported from the **3D**EXPERIENCE Platform by way of a STEP file.

Finite Element Model, FEA (Abaqus)

The CAD geometry was imported into Abaqus/CAE by way of a STEP file.

Figure 14 Imported CAD model

The cortical bone material model was a simple linear elastic model with a Young's modulus of 14,800MPa and an assumed Poisson's ratio of 0.3 [3]. The silicone implant was modeled with an Ogden material model [5], as defined in Table 1, and plotted in Figure 15.

Ogden	
MU1	0.053413 (MPa)
MU2	0.133792 (MPa)
MU3	0.035493 (MPa)
ALPHA1	1.9573
ALPHA2	1.9573
ALPHA3	7.2398
D1	0.00066667 (1/MPa)
D2	1000000 (1/MPa)*
D3	1000000 (1/MPa)*

Table 1 Hyperelastic Ogden material model for Silicone-A, *arbitrarily large

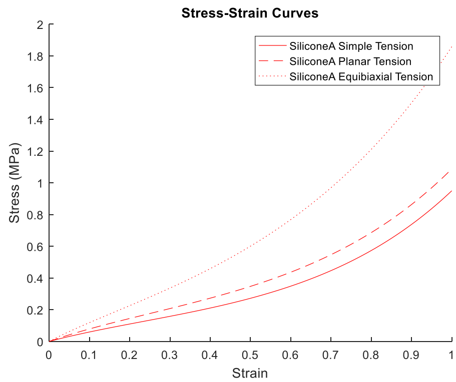

Figure 15 Stress strain curve for Silicone-A

Due to the complex geometry of the bone tissue a hybrid second order tetrahedron mesh (C3D10H) was chosen. A 2mm mesh seed was chosen with a mesh refinement around the stems of 1mm. As the optimization progresses this mesh seed will be reevaluated.

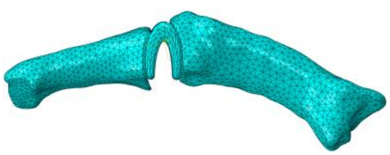

Figure 16 Hybrid second order tetrahedron mesh

Surface to surface contact was defined between the bone and implant for both sides with a slave adjustment to remove overclosure. Surface to surface contact was also defined for self contact of the implant. The distal end of the stem has a kinematic coupling with RP-1 and is rotated in coordinate system where the x-direction is the natural joint bending direction. The proximal end of the stem is fixed.

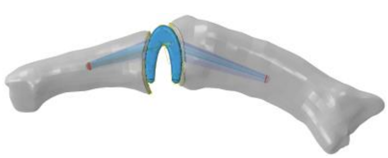

Figure 17 Proximal end fixed, distal end constrained to rotate in defined coordiante system's x-direction

The distal end is rotated to extend the finger by 20° then flexed for 70° and then returned to neutral. Every 10 degrees are associated with 0.1s in this quasi-static analysis. This will consist of 1 fatigue cycle. [4]

Durability Analysis (fe-safe/Rubber)

The two silicone variants reported in Leslie et al (2008) are compared to show how different grades of silicone with similar hyperelastic material properties (herein assumed identical) can influence the fatigue life of a device.

In addition to the hyperelastic properties already given, the fatigue crack growth rate law and initial crack precursor size (ie flaw size) were specified. The Thomas (1958) crack growth rate law was utilized, since the data from the Leslie (2008) results closely fit this model. Both materials have a critical fracture strength T_c of approximately 15 kJ/m^2. The materials differ strikingly, however, in their powerlaw slope F_0, as shown in the plotted crack growth rate curves in Figure 18. Because silicone is an amorphous elastomer, no strain crystallization is specified.

The crack precursor size was calibrated, using fe-safe/rubber's flaw size calibration feature, in the present case to give a similar strain-to-rupture for both silicones – roughly 350%-400%. The crack precursor size of an elastomer reflects the worst case microscopic flaws existing in the material. Such flaws have been shown to arise both from sources intrinsic to the rubber compound (ie polymer and recipe) and from extrinsic sources introduced via mixing (ie dispersion of particulate constituents), contamination or processes that result in porosity (ie inadequate degassing). A review of past studies indicates that precursor sizes in the range from 2 to 200 microns can be expected.

Table 2 gives the values of all crack growth parameters used in the model. The results plotted in Figures 19 and 20 have been computed using fe-safe/Rubber from the given material properties. Figure 19 shows the strain-life curve for each material. Figure 20 shows the Haigh diagram for each material.

Thomas	Silicone-A	Silicone-B
FLAWSIZE	**0.0273 (mm)**	**0.0134 (mm)**
FLAWCRIT	1 (mm)	1 (mm)
RC	5.46e-4 (mm/CYCLE)	5.46e-4 (mm/CYCLE)
TCRITICAL	**15 (kJ/m^2)**	**15 (kJ/m^2)**
F0	**1.29**	**2.54**

Table 2 Hyperelastic Ogden material model for Silicone-A and Silicone-B where the bolded properties indicate differences

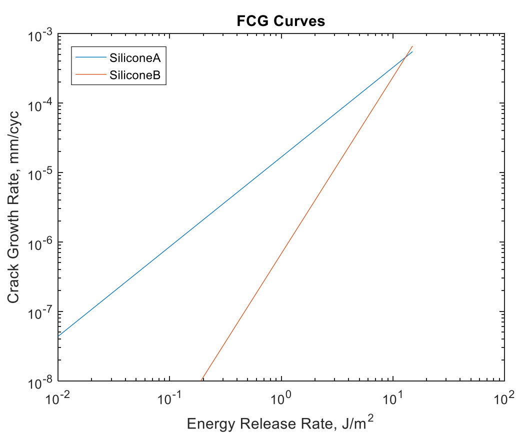

Figure 18 Fatigue Crack Growth curve plots of Silicone-A and Silicone-B

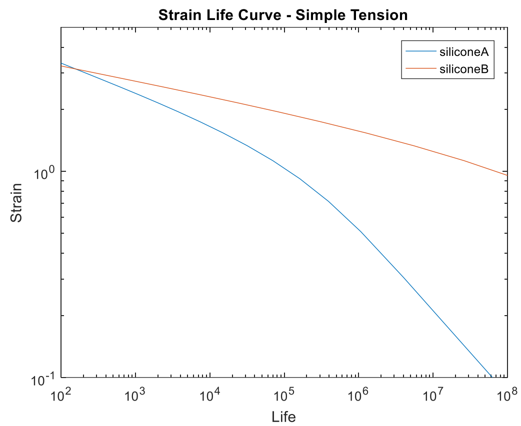

Figure 19 Strain life curve - simple tension of Silicone-A and Silicone-B

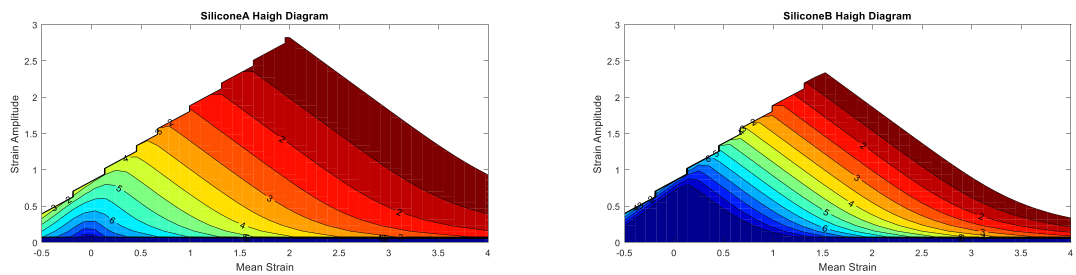

Figure 20 Haigh Diagram Silicone-A and Silicone-B. Blue contours indicate long fatigue life, red contours indicate short life. Contour label values give the base 10 log of the fatigue life (example: 3 = 10^3 = 1000 cycles).

The duty cycle of the implant consists in flexing between the 20° and 70° positions. For purposes of analysis, the motion was discretized in 10° increments. The 6 components of the 3D strain tensor, along with the hydrostatic pressure, were imported to fe-safe/Rubber from the Abaqus ODB file for each element of the model.

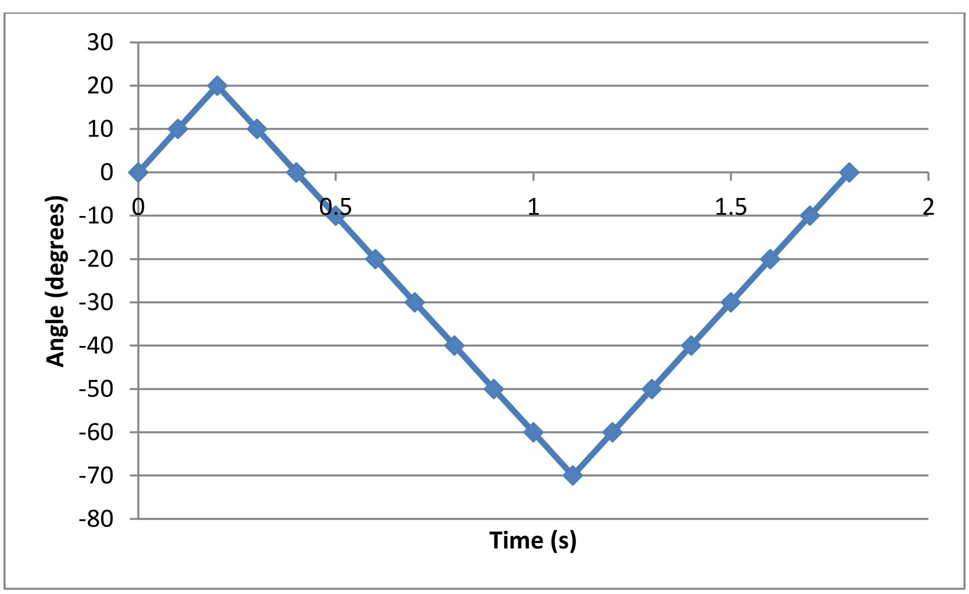

Figure 21 Time history of 1 duty cycle

The strain history in each element of the finite element model is generally multiaxial in nature. Accordingly, fe-safe/Rubber's Critical Plane Analysis is required in order to accurately assess durability. Critical Plane Analysis assumes that a crack precursor may be oriented in any direction, and that therefore a search is required to determine which crack orientation maximizes the rate of crack growth. The crack orientation that maximizes the crack growth simultaneously minimizes fatigue life, and is called the *Critical Plane*. The fatigue life associated with the Critical Plane is computed and reported for each element, and is then plotted to determine locations on the implant where failure will occur.

Results

The initial FEA simulation strain plots are given below for both 20° extension and 70° flexion. Through the fatigue cycle data has been reported for every 10°. In figure 22 the strains have been plotted for the device along with the maximal strain locations for 20° extension and 70° flexion. Figure 23 shows the fatigue life for the device with both silicone-A and Silicone-B. Silicone A has a fatigue life of 1e11 which is higher than the required 1e7, however, with Silicone-B the fatigue life is infinite with no fatigue damage. Also of note is that the maximal strains are not located at the same location as the minimal fatigue life.

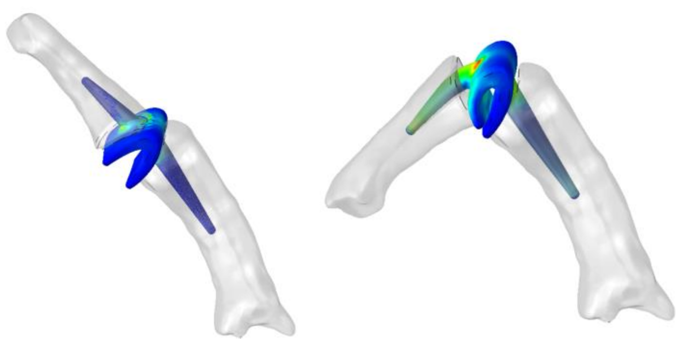

Figure 22 Strain plot under 20° extension and 70° flexion

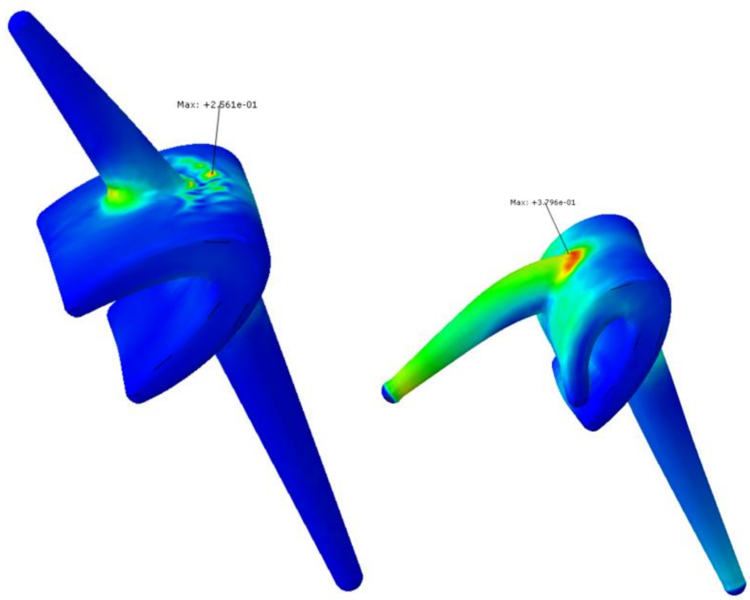

Figure 23 Device only strain plot under 20° extension and 70° flexion with maximal strain locations

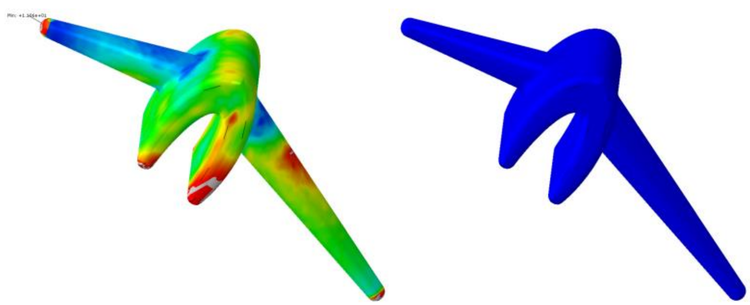

Figure 24 Fatigue life for Silicone-A 11.0578 Loglife-Repeats with minimal life location, Silicone-B has an infinite fatigue life

The predicted direction of crack initiation in the implant can be determined by outputting the damage sphere from fe-safe/Rubber. The damage sphere shows the results of the critical plane analysis on a sphere where each point represents the endpoint of a different unit normal vector. The endpoint of each unit vector is colored according to the fatigue life of the associated crack orientation. The damage sphere is oriented relative to the local element coordinate system, and indicates which loading directions are most responsible for damage occurring at that location in the implant. Based on the damage sphere the fatigue life is dominated by tension in the distal stem.

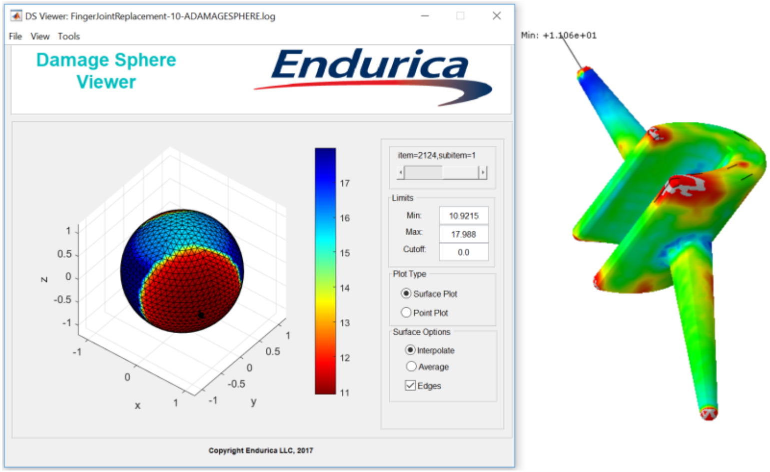

Figure 25 Damage sphere from fe-safe/Rubber: locations of: 20° max strain, 70° max strain and minimum fatigue life

Conclusion

This simulation started with a patient-specific CT scan of the hand which is parsed by density to isolate the bone tissue from the soft tissue. From here CAD geometry was created that matched the neutral hand position of the scan along with a proposed surgical technique. A non-linear finite element model was created that included large deformation, contact and a 3rd order Ogden hyperelastic material properties. These results were imported into the fe-safe/Rubber durability calculation with a non-crystallizing Thomas law. From here a non-parametric shape optimization was performed to increase the device's fatigue life.

References

1. Swanson Surgical Technique http://www.wmtemedia.com/ProductFiles/Files/PDFs/010500_EN_HR_LE.pdf
2. Visible Korean http://vkh3.kisti.re.kr/?q=node/24
3. Cortical bone modulus https://www.ncbi.nlm.nih.gov/pubmed/8429054
4. Support for 10 million cycles through 90 degrees of flex. https://www.accessdata.fda.gov/cdrh_docs/pdf/K970544.pdf
5. Silicone material properties http://www.sciencedirect.com/science/article/pii/S2214963514000480
6. Leslie, Laura, Stephen Kukureka, and D. E. T. Shepherd. "Crack growth of medical-grade silicone using pure shear tests." *Proceedings of the Institution of Mechanical Engineers, Part H: Journal of Engineering in Medicine* 222, no. 6 (2008): 977-982.
7. Thomas, A. G. "Rupture of rubber. V. Cut growth in natural rubber vulcanizates." *Journal of Polymer Science Part A: Polymer Chemistry* 31, no. 123 (1958): 467-480.

Acknowledgements

1. Kerim Genc and Thomas Spirka (Synopsys) for providing processed CT data and scan visualization guidance.
2. Will Mars and Mark Bauman (Endurica) for providing material properties and fatigue modelling guidance.